Earth Syst. Sci. Data, 11, 741–759, 2019
https://doi.org/10.5194/essd-11-741-2019

Open Access Earth System Science Data

A database of marine and terrestrial radiogenic Nd and Sr isotopes for tracing earth-surface processes

Cécile L. Blanchet[1,a]

[1]Department of Geosciences, Freie Universität Berlin, Berlin, Germany
[a]now at: GFZ German Research Centre for Geosciences, Climate Dynamics and Landscape Evolution, Potsdam, Germany

Correspondence: Cécile L. Blanchet (blanchet@gfz-potsdam.de)

Received: 12 September 2018 – Discussion started: 8 October 2018
Revised: 18 April 2019 – Accepted: 24 April 2019 – Published: 24 May 2019

Abstract. The database presented here contains radiogenic neodymium and strontium isotope ratios measured on both terrestrial and marine sediments. The main purpose of this dataset is to help assess sediment provenance and transport processes for various time intervals. This can be achieved by either mapping sediment isotopic signature and/or fingerprinting source areas using statistical tools.

The database has been built by incorporating data from the literature and the SedDB database and harmonizing the metadata, especially units and geographical coordinates. The original data were processed in three steps. Firstly, specific attention has been devoted to providing geographical coordinates to each sample in order to be able to map the data. When available, the original geographical coordinates from the reference (generally DMS coordinates) were transferred into the decimal degrees system. When coordinates were not provided, an approximate location was derived from available information in the original publication. Secondly, all samples were assigned a set of standardized criteria that help split the dataset into specific categories. For instance, samples were distinguished according to their location ("Region", "Sub-region" and "Location" that relate to locations at continental to city or river scale) or the sample type (terrestrial samples – "aerosols", "soil sediments", "river sediments", "rocks" – or marine samples – "marine sediment" or "trap sample"). Finally, samples were distinguished according to their deposition age, which allowed us to compute average values for specific time intervals.

Graphical examples illustrating the functionality of the database are presented and the validity of the process was tested by comparing the results with published data. The dataset will be updated bi-annually in order to add more data points to increase the sampling density or provide new types of samples (e.g. seawater signature) and/or integrate additional information regarding the samples. It is publicly available (under CC4.0-BY Licence) from the GFZ data management service at https://doi.org/10.5880/GFZ.4.3.2019.001.

1 Introduction

A large amount of sediments is deposited by rivers and winds on continental margins and in the deeper parts of marine basins. These deposits constitute valuable climatic archives that are used in conjunction with terrestrial records and model outputs to better understand the climate–earth system. In that general context, the radiogenic isotopes of neodymium (Nd) and strontium (Sr) measured in marine sediments have proven a powerful tool to determine their origin and their mode of transportation (i.e. fluvial or aeolian), related to climatic fluctuations (Frank, 2002). Neodymium isotope ratios are generally used to fingerprint provenance changes, as continental rocks have specific Nd isotopic signatures that are preserved during transportation and burial of sediments. Strontium isotope ratios are also sensitive provenance tracers, but their original signature can be modified by weathering processes in the source area as well as grain-size sorting during sediment transportation. In conjunction with

Nd isotopes, Sr isotope ratios therefore provide additional information on earth-surface processes, such as changes in hydrological conditions, vegetation cover and modes of sediment transport.

The value of compiling Nd and Sr radioisotope datasets has already been demonstrated by pioneering studies that investigated sediment generation and transport processes (Goldstein et al., 1984; Goldstein and O'Nions, 1981; Grousset et al., 1988, 1990, 1992). More recently, several data compilations were used to trace submarine sediment transport processes or boundary exchanges (Jeandel et al., 2007; Krom et al., 1999b; Tachikawa et al., 2017; Weldeab et al., 2002a) and fingerprint continental source areas (e.g. Padoan et al., 2011, for the Nile River basin and Scheuvens et al., 2013, for northern Africa). The sedimentary database for geochemical analyses, SedDB, which is hosted on the EarthChem platform, provides a large number of data for Nd and Sr isotopes (http://www.earthchem.org/seddb, last access: 20 February 2019). This useful instrument allows us to sort data per type of analysis, age and location (among other criteria), but has been put on hold since 2013 and is therefore not up to date. Consequently, there is at present no combined dataset that allows us to evaluate the contribution of specific sources to the sedimentary records, and authors use parts of these datasets arbitrarily, based on their geographical relevance, together with their own discrete measurements (Blanchet et al., 2013; Castañeda et al., 2016; Revel et al., 2010; Wu et al., 2016). The lack of a comprehensive dataset therefore hinders the possibility of obtaining statistically significant estimations of source contribution to the sediments and the use of harmonized identifiers for provenance.

This paper introduces a compilation of published and unpublished data, which includes an integrated filtering system using criteria to subset the dataset. In addition to present-day measurements provided by the previously cited and additional studies, specific time intervals were selected in order to plot and analyse paleo-data in view of present-day values. This dataset is envisaged as an evolutive tool that will be bi-annually updated and will remain in the public domain. Other relevant proxies and/or filtering criteria can be implemented in collaboration with peers.

The functionality of the database will be demonstrated by presenting some examples. Plotting has been realized with the R freeware (R Core Team, 2013), and R scripts are also published to allow other users to subset and plot the data (Blanchet, 2018a, b).

2 Methods

2.1 Input data

The database has been built by incorporating data from the literature and the SedDB database and harmonizing the metadata, especially units and geographical coordinates. An overview of the input data is shown in Table 1.

In a first iteration (published in September 2018, https://doi.org/10.5880/GFZ.5.2.2018.001), the pre-existing datasets from Padoan et al. (2011) and Scheuvens et al. (2013) were used (which included datasets from Krom et al., 1999b, a, and Weldeab et al., 2002a, b). The focus of these studies is different (river runoff and dust characterization respectively), but they are complementary and provide a large number of data (86 and 192 data points respectively). Second, 70 points were retrieved from the SedDB database, which could be identified as core tops and siliciclastic fraction (criteria set for Africa and Europe – 40° S–55° N; 35° W–60° N). Finally, a literature search has been conducted in order to add discrete samples that were not part of the previously cited compilations (276 data points). Data were collected from 48 different references with 631 data points in total (Table 1).

In a second iteration (published in April 2019, https://doi.org/10.5880/GFZ.4.3.2019.001), data compiled by Jeandel et al. (2007) have been added to the database, which provided an additional 222 data points and extended the geographical extent towards a global coverage (Table 1). Then, 116 points were retrieved from the SedDB database, which could be identified as core tops and siliciclastic fraction (global geographical extent). Based on external contribution (addition proposed by colleagues), author contribution (data published and provided by first or co-authors) or literature search, another 561 data points were added. The locations of these new samples are shown on maps in Fig. 1b.

The database contains samples on which either the Nd or Sr (or both) radiogenic isotope ratios were measured and expressed as $\varepsilon_{Nd(0)}$ and $^{87}Sr/^{86}Sr$. The notation $\varepsilon_{Nd(0)}$ is widely used and is calculated as

$$\varepsilon_{Nd(0)} = \left[\left({}^{143}Nd/{}^{144}Nd \right)_{sample} \Big/ \left({}^{143}Nd/{}^{144}Nd \right)_{CHUR} - 1 \right] \cdot 10\,000,$$

where CHUR stands for chondritic uniform reservoir and has a $^{143}Nd/^{144}Nd$ ratio of 0.512638 (Bouvier et al., 2008; Jacobsen and Wasserburg, 1980). When possible, additional variables were incorporated, such as the raw $^{143}Nd/^{144}Nd$ isotope ratio and the concentration in Sr and/or Nd in parts per million (ppm). As shown by Cole et al. (2009), sedimentary Nd and Sr concentrations can provide valuable clues for paleo-environmental interpretations.

2.2 Data processing

The original data were then processed in three steps, as shown in Table 1. Firstly, specific attention has been devoted to providing geographical coordinates to each sample in order to be able to map the data (cf. Fig. 1). When

Table 1. Data input sources and type of data provided in two iterations of the database (September 2018 and April 2019). The first column shows the input sources (Padoan et al., 2011; Scheuvens et al., 2013).

Source	Characteristics	Data characteristics	Attribution/ harmonization of coordinates	Attribution of sorting criteria	Determination of specific time interval	Number of data points
First iteration (September 2018)						
Padoan	Research article	River sed.	YES	YES	NO	86
Scheuvens	Review article	Aerosols, marine sed., river sed., soils, trap sample	YES	YES	YES	192
SedDB[a]	Database	Marine sed.	YES	YES	YES	70
Literature search[b]	Peer-reviewed publications	River sed., aerosols, rocks, marine sed., soil sed., trap sample, foraminifera	YES	YES	YES	342
Own data[c]	Own research articles and own measurements	River sed., aerosols, rocks, marine sed., soil sed.	NO	YES	YES	7
Total first iteration						631
Second iteration (April 2019)						
Jeandel	Research article	River sed., aerosols, rocks, marine sed., soil sed.	NO	YES	YES	222
SedDB[a]	Database	Sedimentary database	YES	YES	YES	116
Literature search[b]	Peer-reviewed publications	River sed., aerosols, rocks, marine sed., soil sed., trap sample, foraminifera	YES	YES	YES	342
External contribution[d]	Peer-reviewed publications	Aerosols, rocks, marine sed., soil sed.	YES	YES	YES	194
Author contribution[e]	Peer-reviewed publications	River sed., marine sed.	YES	YES	YES	25
Total second iteration						899
Grand total						1530

[a] SedDB at http://www.earthchem.org/seddb (last access: 20 February 2019). [b] Reference list for the dataset available at Blanchet (2019). [c] Own data from Blanchet et al. (2014). [d] Contribution from colleagues. [e] Contribution from first or co-author. Indications of the type of source and the characteristics of the data retrieved are provided. The data were then submitted to three processes: sorting criteria were attributed to all the samples, a homogenous geographical location (coordinates in decimal degrees) was attributed to some samples, and the isotopic values of specific time intervals were determined when possible (see Sect. 2 and Table 2 for further information).

available, the original geographical coordinates from the reference (generally DMS coordinates, with a different precision standard) were transferred into the decimal degrees system. When coordinates were not provided, an approximate location for the samples was estimated from available information in the original publication. Maps or mention of actual locations (e.g. cities) were used to determine their geographical location using online coordinate finders (e.g. https://www.latlong.net/, last access: 20 February 2019).

All samples were then assigned a set of standardized criteria that help split the dataset into specific categories (Table 1). Samples were attributed criteria related to their location. The "Region" category provides a general sorting at continental or oceanic scale (e.g. "Mediterranean", "Atlantic", "Africa", "Europe") and the "Sub-region" category allows us to select only specific areas at oceanic sub-basins or country level (e.g. Mediterranean sub-basins or African countries). A third category, "Location", permits us to select specific areas (e.g. cities) or entities such as river basins or potential source areas (PSAs) for dust production as defined in Scheuvens et al. (2013) (Fig. 1a). Criteria were also defined in order to select specific types of samples: terrestrial samples ("aerosols", "soil sediments", "river sediments", "bivalves", "rocks") or marine samples ("marine sediment", "trap sample") (Fig. 1). When available, the grain-size fraction on which the measurements were carried out (bulk or fraction in µm) was re-

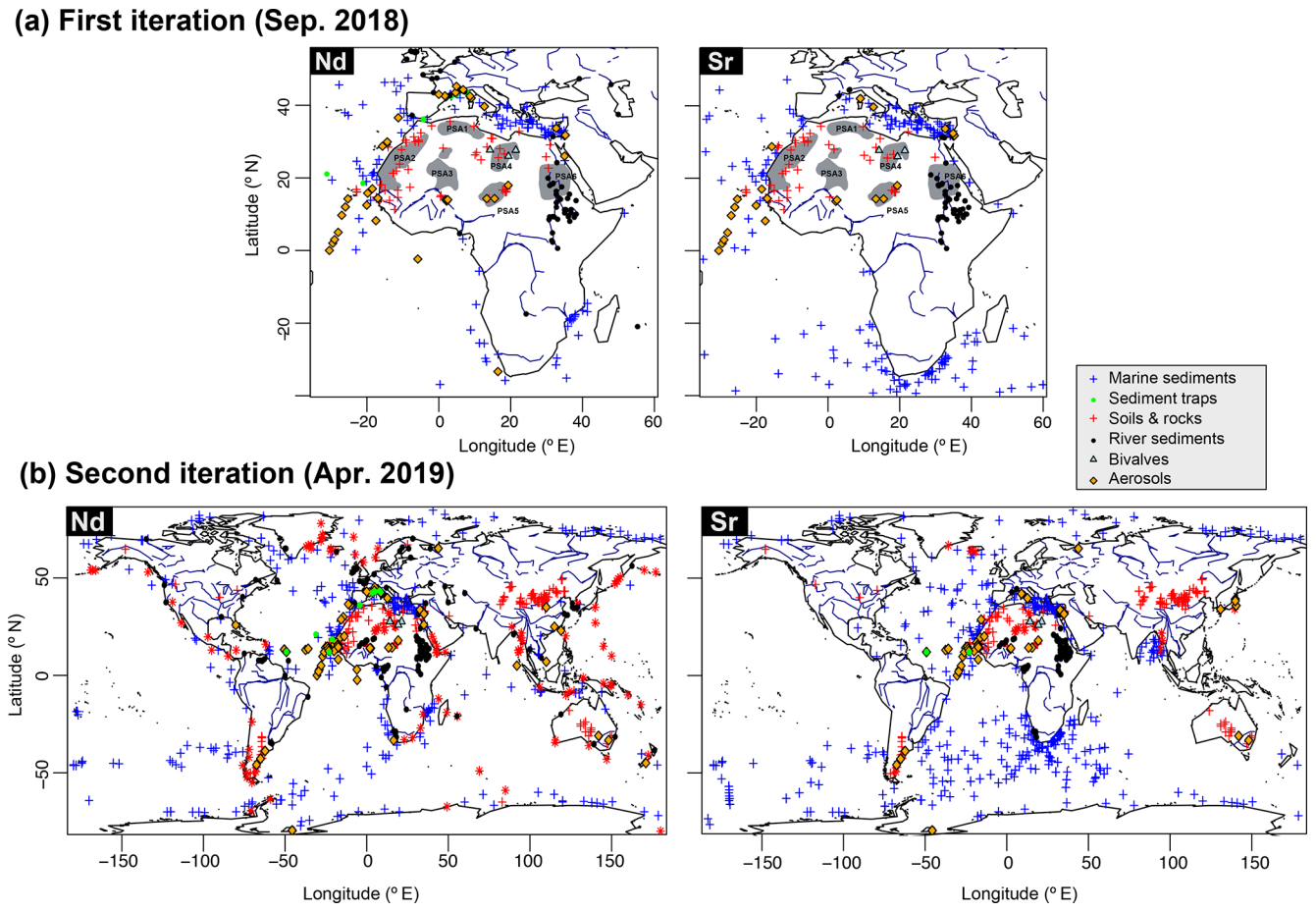

Figure 1. Overview of the location of samples assembled in the database for neodymium and strontium isotope ratios. The sample types are indicated by different markers: blue crosses for marine sediments, green dots for sediment traps, red crosses for soil samples, black dots for river sediments (river banks or particulate matter), blue triangles for fossil bivalves (Osborne et al., 2008) and yellow diamonds for deposited dust samples. **(a)** Dataset assembled for the first iteration published in September 2018. The African PSAs are indicated as grey underlines and were redrawn from Scheuvens et al. (2013). **(b)** Dataset assembled for the second iteration published in April 2019. A complete list of references is provided in the Supplement to the main dataset (http://doi.org/10.5880/GFZ.4.3.2019.001).

ported, as such information can be useful for tracing specific transportation modes (Blanchet et al., 2013).

Third, samples were discriminated according to their age, and average values were computed for specific time intervals (Table 2). Most terrestrial samples are categorized as present-day samples, but marine samples were sorted according to their age.

- Labelled "P" (present-day): I report here only surface seafloor samples for present-day sedimentation (i.e. generally core top, the upper centimetre or past millennium). Sediment core samples that were collected below 1 cm or that were older than 1000 years were not reported here as their value might be significantly different than the present-day value, due to different climatic and oceanographic conditions (e.g. see values at 3–4 ka in Blanchet et al., 2014).
- Labelled "S1, S3, S4, S5, S6" (sapropels): this refers to samples from the well-defined sapropel layers in the Mediterranean. Climatic and oceanic conditions are known to be radically different during these time intervals (with large freshwater delivery and low oxygen content in deeper parts of the Mediterranean Basin), which led to the occurrence of specific depositional environments (Rossignol-Strick, 1985). These layers are generally visible (distinct black to grey-coloured sediments) in the sediment records, and their extent is defined by specific geochemical tracers, such as the total organic carbon content or the barium-to-aluminium ratio (De Lange et al., 2008). Using these markers and indications from the original publication, an average for these specific layers was calculated (used as a single value in the dataset). The depth or age interval used for the calculation, as well as the number of sample and ob-

Table 2. Identification of specific time intervals (sapropel layers and last glacial maximum) in marine sediments for the first iteration of the database. Headers from left to right: Label: name of the sediment core; Time interval: sapropel layers S1, S3, S4, S5 and S6 and last glacial maximum LGM; Core depth interval (cm) and corresponding Duration (kyr); n: number of samples; averages and standard deviations (2σ) for Sr and Nd isotope ratios (with Nd isotopes expressed as $\varepsilon_{Nd(0)}$); Identifier: measurement or method used to determine the extent of the specific time interval; Ref.: reference publications. 1: Box et al. (2011), 2: Blanchet et al. (2019), 3: Krom et al. (1999a), 4: Freydier et al. (2001), 5: Jung et al. (2004), 6: Krom et al. (2002), 7: Wu et al. (2016), 8: Castañeda et al. (2016), 9: Stein et al. (2007), 10: Palchan et al. (2013), 11: Révillon et al. (2011), 12: Revel et al. (2015), 13: Revel et al. (2010, 2014), 14: Cole et al. (2009), 15: Blanchet et al. (2014), 16: Revel-Rolland et al. (2006), 17: Grousset et al. (1998), 18: Noble et al. (2012), 19: Franzese et al. (2009), 20: Hemming et al. (2007), 21: Revel et al. (1996), 22: Colin et al. (1999), 23: Roy et al. (2007), 24: Franzese et al. (2006), 25: Weldeab et al. (2002b).

Label	Time interval	Core depth interval (cm)	Duration (kyr)	n	$^{87}Sr/^{86}Sr$	2σ	$\varepsilon_{Nd(0)}$	2σ	Identifier	Ref.
9501	S1	64–87	6.49–9.93	12	0.71072	0.00036	NA	NA	geochemical (TOC, Ba/Al)	1
9509	S1	100–180	6.17–9.97	13	0.70952	0.00032	NA	NA	geochemical (TOC, Ba/Al)	
64PE349-8	S1	20–30	5.04–8.32	3	0.71608	0.00101	−10.65	0.98	visual, geochemical (TOC, Ba/Al)	2
ABC26	S1	22.6–25.8		3	0.71483	0.00266	NA	NA	Geochemical (TOC)	3
BC07	S1	15.25–36.25		8	0.71122	0.00017	−8.46	0.36	Geochemical (Ba/Al)	4
BC19	S1	23.25–30.25		5	0.71179	0.00054	−8.16	0.30	Geochemical (Ba/Al)	
BC19	S1	27–35		3	0.70978	0.00013	NA	NA	Geochemical (TOC)	3
BC3	S1	12.8–21.2		5	0.71604	0.00075	−10.82	0.26	Geochemical (Ba/Al)	4
Core NIOP 905 P	S1		6.43–9.53	81	0.71426	0.00032	−5.91	0.25	Age – African Humid Period	5
Cores s-21	S1	Determined in publication	> 6	4	0.70880	–	NA	NA	Age – African Humid Period	6
CP10BC	S1	21.25–34.75	6.2–9.6	16	0.71604	0.00104	−11.17	0.30	visual, geochemical (TOC, Ba/Al)	7
GeoB7702-3	S1	2.46–2.58	8.66–9.88	2	0.70900	0.00000	−4.64	0.33	geochemical (biomarkers)	8
KC01	S1	11.8–13.0		4	0.71372	0.00126	NA	NA	Geochemical (TOC)	3
KL11	S1	64–65	6	1	0.70831	NA			Age – African Humid Period	9
KL15	S1	41–42	6.6	1	0.70968	NA			Age – African Humid Period	
KL23	S1	Determined in publication	NA	NA	0.7111450	NA	−5.69	NA	Age – LGM	10
KSGC31-671	S1	671	8.94	1	0.71716	NA	−10.9		Age – African Humid Period	11
MC12	S1	23.1–27.1		2	0.71317	0.00074	NA	NA	Geochemical (TOC)	3
MD04-2622	S1	113–121	9.9–10.0	2	0.70909	0.00008	−6.16	0.03	visual, geochemical (TOC, Ba/Al)	12
MD04-2627	S1	75–111	6.01–10.27	20			−3.81	0.67	visual, geochemical (TOC, Ba/Al)	
MS27PT	S1	23–294	6.15–14.26	55	0.70860	0.00105	−4.99	1.10	visual, geochemical (TOC, Ba/Al)	12, 13
ODP Leg 108, Site 658C	S1	1.35–2.02	6.06–9.82	19	0.71653	0.00125	−14.33	0.23	Age – African Humid Period	14
P362/2-33	S1	50–551	6.11–9.53	22	0.70876	0.00126	−3.80	0.71	visual, geochemical (TOC, Ba/Al)	15

Table 2. Continued.

Label	Time interval	Core depth interval (cm)	Duration (kyr)	n	$^{87}Sr/^{86}Sr$	2σ	$\varepsilon_{Nd(0)}$	2σ	Identifier	Ref.
SL114	S1	24.05–34.05	NA	4	0.71607	0.00058	−10.35	0.31	Geochemical (Ba/Al)	4
Stn 20	S1	19.5–24.5	NA	3	0.71408	0.00305	NA	NA	Geochemical (TOC)	3
UM35	S1	19.25–26.25	NA	5	0.71524	0.00125	NA	NA	Geochemical (TOC)	
UM42	S1	22.15–27.65	NA	6	0.71581	0.00060	−11.48	0.52	Geochemical (Ba/Al)	4
Brown's Creek (BC-1 0.15 cm)	< 8.4 ka	Determined in publication	NA	NA	0.714161	NA	−8	NA	Age	6
Core E26.1 (E1-1 cm)	∼ 4.5 ka	Determined in publication	NA	NA	0.711128	NA	−5.6	NA	Age – African Humid Period	
28	LGM	Determined in publication	NA		0.72044		−12.40		Age – LGM	17
29	LGM	Determined in publication	NA		0.71744		−13.70		Age – LGM	
31	LGM	Determined in publication	NA		0.71744		−13.30		Age – LGM	
32	LGM	Determined in publication	NA		0.72093		−13.10		Age – LGM	
177-1088B	LGM	Determined in publication	NA	NA	0.7121000	NA	−7.90	NA	Age – LGM	18
177-1089A	LGM	Determined in publication	NA	NA	0.7154900	NA	−9.10	NA	Age – LGM	
Brown's Creek (BC-2 0.70 cm)	LGM	Determined in publication	NA	NA	0.714385	NA	−8	NA	Age – LGM	16
CD154-02-3K	LGM	Determined in publication	NA	NA	0.7307500	NA	NA	NA	Age – LGM	19
CD154-06-6PK	LGM	Determined in publication	NA	NA	0.7247600	NA	NA	NA	Age – LGM	
CD154-09-9PK	LGM	Determined in publication	NA	NA	0.7225800	NA	NA	NA	Age – LGM	
CD154-13-12K	LGM	Determined in publication	NA	NA	0.7205400	NA	NA	NA	Age – LGM	
CD154-15-12PK	LGM	Determined in publication	NA	NA	0.7189300	NA	NA	NA	Age – LGM	
CD154-15-13K	LGM	Determined in publication	NA	NA	0.7163200	NA	NA	NA	Age – LGM	
CD154-15-14K	LGM	Determined in publication	NA	NA	0.7159200	NA	NA	NA	Age – LGM	
CD154-16-15K	LGM	Determined in publication	NA	NA	0.7182000	NA	NA	NA	Age – LGM	
Core E26.1 (E8-35 cm)	LGM	Determined in publication	NA	NA	0.711945	NA	−4.6	NA	Age – LGM	16
E11-2	LGM	Determined in publication	NA	NA	0.7106510	NA	NA	NA	Age – LGM	20
E17-9	LGM	Determined in publication	NA	NA	0.7108550	NA	NA	NA	Age – LGM	
E20-10	LGM	Determined in publication	NA	NA	0.7106080	NA	NA	NA	Age – LGM	
E20-10	LGM	Determined in publication	NA	NA	0.7089660	NA	NA	NA	Age – LGM	
GC027	LGM	Determined in publication	NA	NA	0.7201400	NA	−8.70	NA	Age – LGM	18
K02	LGM	Determined in publication	NA		0.72308		−17.80		Age – LGM	17
K11	LGM	Determined in publication	NA		0.71699		−17.90		Age – LGM	

Table 2. Continued.

Label	Time interval	Core depth interval (cm)	Duration (kyr)	n	$^{87}Sr/^{86}Sr$	2σ	$\varepsilon_{Nd(0)}$	2σ	Identifier	Ref.
K15	LGM	Determined in publication	NA		0.71904		−19.50		Age – LGM	17
K17d	LGM	Determined in publication	NA		0.71632				Age – LGM	
K20b	LGM	Determined in publication	NA		0.71933		−14.10		Age – LGM	
11 KC088	LGM	Determined in publication	NA	NA	0.7156800	NA	−7.40	NA	Age – LGM	18
KC089	LGM	Determined in publication	NA	NA	0.7195100	NA	−8.50	NA	Age – LGM	
KL23	LGM	Determined in publication	NA	NA	0.7111285	NA	−5.68	NA	Age – LGM	10
KS-7925	LGM	Determined in publication	NA	NA	0.7154220	NA	NA	NA	Age – LGM	21
KS-7929	LGM	Determined in publication	NA	NA	0.7235340	NA	−10.80	NA	Age – LGM	
Lake Eyre (Shelly Island unit)	LGM	Determined in publication	NA	NA	0.70926	NA	−3	NA	Age – LGM	16
MD77-169	LGM	158	Determined in publication	NA	0.71669	NA	−10.6	NA	Age determination	22
MD77-171	LGM	265	Determined in publication	NA	0.71332	NA	−8.8	NA	Age determination	
MD77-176	LGM	590	Determined in publication	NA	0.71777	NA	−8.4	NA	Age determination	
MD77-178	LGM	240	Determined in publication	NA	0.71613	NA	−7.0	NA	Age determination	
MD77-179	LGM	41	Determined in publication	NA	0.72101	NA	−10.7	NA	Age determination	
MD77-180	LGM	200	Determined in publication	NA	0.72315	NA	−11.0	NA	Age determination	
MD77-181	LGM	165	Determined in publication	NA	0.72135	NA	−10.2	NA	Age determination	
MD77-183	LGM	175	Determined in publication	NA	0.71914	NA	−8.6	NA	Age determination	
MD77-186	LGM	240	Determined in publication	NA	0.71683	NA	−10.2	NA	Age determination	
NBP9802_3GC1	LGM	Determined in publication	NA	NA	0.7140920	NA	NA	NA	Age – LGM	20
NBP9802_4GC1	LGM	Determined in publication	NA	NA	0.7119520	NA	−2.70	NA	Age – LGM	20, 23
NBP9802_5GC1	LGM	Determined in publication	NA	NA	0.7107350	NA	NA	NA	Age – LGM	20
NBP9802_6PC1	LGM	Determined in publication	NA	NA	0.7151280	NA	NA	NA	Age – LGM	
NBP9802_9PC1	LGM	Determined in publication	NA	NA	0.7121280	NA	NA	NA	Age – LGM	
ODP 645	LGM	Determined in publication	NA	NA	0.7322540	NA	−27.00	NA	Age – LGM	21
Orgon KS9	LGM	Determined in publication	NA	NA	0.7293380	NA	−20.10	NA	Age – LGM	
PS2819-1	LGM	Determined in publication	NA	NA	0.7122600	NA	−9.90	NA	Age – LGM	18
PS2820-1	LGM	Determined in publication	NA	NA	0.7128800	NA	−10.00	NA	Age – LGM	
RC11-46	LGM	Determined in publication	NA	NA	0.7091000	NA	NA	NA	Age – LGM	24
RC11-76	LGM	Determined in publication	NA	NA	0.7108000	NA	NA	NA	Age – LGM	
RC11-77	LGM	Determined in publication	NA	NA	0.7093600	NA	−4.48	NA	Age – LGM	

Table 2. Continued.

Label	Time interval	Core depth interval (cm)	Duration (kyr)	n	$^{87}Sr/^{86}Sr$	2σ	$\varepsilon_{Nd(0)}$	2σ	Identifier	Ref.
RC11-78	LGM	Determined in publication	NA	NA	0.7107000	NA	NA	NA	Age – LGM	
RC11-80	LGM	Determined in publication	NA	NA	0.7101100	NA	−5.72	NA	Age – LGM	24
RC11-83	LGM	Determined in publication	NA	NA	0.7175	NA	NA	NA	Age – LGM	
RC11-86	LGM	Determined in publication	NA	NA	0.7269600	NA	−10.17	NA	Age – LGM	
RC11-87	LGM	Determined in publication	NA	NA	0.7161400	NA	NA	NA	Age – LGM	19
RC11-94	LGM	Determined in publication	NA	NA	0.7106000	NA	NA	NA	Age – LGM	
RC11-95	LGM	Determined in publication	NA	NA	0.7099000	NA	NA	NA	Age – LGM	24
RC11-96	LGM	Determined in publication	NA	NA	0.7096000	NA	NA	NA	Age – LGM	
RC11-119	LGM	Determined in publication	NA	NA	0.7131130	NA	NA	NA	Age – LGM	
RC11-46	LGM	300	Determined in publication	NA	0.7090810	NA	NA	NA	Age – LGM	
RC11-76	LGM	438–439	Determined in publication	NA	0.7108050	NA	NA	NA	Age – LGM	20
RC11-77	LGM	200	Determined in publication	NA	0.7093720	NA	NA	NA	Age – LGM	
RC11-80	LGM	95	Determined in publication	NA	0.7101190	NA	NA	NA	Age – LGM	
RC11-94	LGM	480	Determined in publication	NA	0.7105790	NA	NA	NA	Age – LGM	
RC11-95	LGM	99–100	Determined in publication	NA	0.7098850	NA	NA	NA	Age – LGM	
RC11-96	LGM	100–101	Determined in publication	NA	0.7095820	NA	NA	NA	Age – LGM	
RC12-289	LGM	Determined in publication	NA	NA	0.7092500	NA	−4.73	NA	Age – LGM	24
RC12-339	LGM	101	Determined in publication	NA	0.71574	NA	−10.1	NA	Age determination	
RC12-340	LGM	70	Determined in publication	NA	0.71789	NA	−9.5	NA	Age determination	22
RC12-341	LGM	60	Determined in publication	NA	0.71799	NA	−8.6	NA	Age determination	
RC12-344	LGM	320	Determined in publication	NA	0.7223	NA	−11.5	NA	Age determination	
RC12-289	LGM	Determined in publication	NA	NA	0.7092650	NA	NA	NA	Age – LGM	20
RC13-227	LGM	Determined in publication	NA	NA	0.7210800	NA	−10.12	NA	Age – LGM	
RC13-229	LGM	Determined in publication	NA	NA	0.7185200	NA	−9.43	NA	Age – LGM	
RC13-243	LGM	Determined in publication	NA	NA	0.7130500	NA	−6.43	NA	Age – LGM	
RC13-251	LGM	Determined in publication	NA	NA	0.7109400	NA	−5.90	NA	Age – LGM	24
RC13-254	LGM	Determined in publication	NA	NA	0.7125000	NA	NA	NA	Age – LGM	
RC13-255	LGM	Determined in publication	NA	NA	0.7100100	NA	−4.83	NA	Age – LGM	
RC13-256	LGM	Determined in publication	NA	NA	0.7090000	NA	NA	NA	Age – LGM	

Table 2. Continued.

Label	Time interval	Core depth interval (cm)	Duration (kyr)	n	$^{87}Sr/^{86}Sr$	2σ	$\varepsilon_{Nd(0)}$	2σ	Identifier	Ref.
RC13-251	LGM	18–19	Determined in publication	NA	0.7109540	NA	NA	NA	Age – LGM	20
RC13-254	LGM	Determined in publication	NA	NA	0.7124550	NA	NA	NA	Age – LGM	
RC13-255	LGM	Determined in publication	NA	NA	0.7080340	NA	NA	NA	Age – LGM	
RC13-256	LGM	Determined in publication	NA	NA	0.7089900	NA	NA	NA	Age – LGM	
RC14-11	LGM	Determined in publication	NA	NA	0.7102000	NA	NA	NA	Age – LGM	24
RC14-3	LGM	Determined in publication	NA	NA	0.7166800	NA	NA	NA	Age – LGM	18
RC14-11	LGM	79–80	Determined in publication	NA	0.7102420	NA	NA	NA	Age – LGM	20
RC15-98	LGM	Determined in publication	NA	NA	0.7098000	NA	NA	NA	Age – LGM	24
RC17-53	LGM	Determined in publication	NA	NA	0.7118000	NA	NA	NA	Age – LGM	
RC17-58	LGM	Determined in publication	NA	NA	0.7107000	NA	NA	NA	Age – LGM	
RC17-60	LGM	Determined in publication	NA	NA	0.7140000	NA	NA	NA	Age – LGM	
RC17-61	LGM	Determined in publication	NA	NA	0.7109000	NA	NA	NA	Age – LGM	
RC17-69	LGM	Determined in publication	NA	NA	0.7239100	NA	−11.72	NA	Age – LGM	
RC17-53	LGM	Determined in publication	NA	NA	0.7117680	NA	NA	NA	Age – LGM	20
RC17-61	LGM	Determined in publication	NA	NA	0.7109310	NA	NA	NA	Age – LGM	
RC8-19	LGM	Determined in publication	NA	NA	0.7119000	NA	NA	NA	Age – LGM	24
SU-9011	LGM	Determined in publication	NA	NA	0.7201630	NA	NA	NA	Age – LGM	21
SU-9033	LGM	Determined in publication	NA	NA	0.7077340	NA	NA	NA	Age – LGM	
SU-9038	LGM	Determined in publication	NA	NA	0.7282190	NA	NA	NA	Age – LGM	
SU9008	LGM	Determined in publication	NA	NA	0.7233080	NA	−18.10	NA	Age – LGM	
TPC288	LGM	Determined in publication	NA	NA	0.7094000	NA	−4.80	NA	Age – LGM	18
TPC290	LGM	Determined in publication	NA	NA	0.7072700	NA	−3.50	NA	Age – LGM	
V24-203	LGM	179–180	Determined in publication	NA	0.7062170	NA	NA	NA	Age – LGM	20
V29-84	LGM	120	Determined in publication	NA	0.7125210	NA	NA	NA	Age – LGM	
V29-86	LGM	181–182	Determined in publication	NA	0.7085070	NA	NA	NA	Age – LGM	
VM14-77	LGM	Determined in publication	NA	NA	0.7286100	NA	−16.08	NA	Age – LGM	24
VM16-53	LGM	Determined in publication	NA	NA	0.7185300	NA	NA	NA	Age – LGM	18
VM19-214	LGM	Determined in publication	NA	NA	0.7336900	NA	−14.78	NA	Age – LGM	24
VM19-224	LGM	Determined in publication	NA	NA	0.7169600	NA	NA	NA	Age – LGM	18

Table 2. Continued.

Label	Time interval	Core depth interval (cm)	Duration (kyr)	n	$^{87}Sr/^{86}Sr$	2σ	$\varepsilon_{Nd(0)}$	2σ	Identifier	Ref.
VM19-240	LGM	Determined in publication	NA	NA	0.7230700	NA	−9.65	NA	Age – LGM	24
VM20-201	LGM	Determined in publication	NA	NA	0.7192300	NA	NA	NA	Age – LGM	18
VM22-189	LGM	Determined in publication	NA		0.71805		−13.80		Age – LGM	17
VM22-196	LGM	Determined in publication	NA		0.71991		−18.30		Age – LGM	
VM24-203	LGM	Determined in publication	NA	NA	0.7062000	NA	NA	NA	Age – LGM	24
VM24-231	LGM	Determined in publication	NA	NA	0.7098000	NA	NA	NA	Age – LGM	
VM27-175	LGM	Determined in publication	NA		0.71848		−15.90		Age – LGM	17
VM29-15	LGM	72	Determined in publication	NA	0.71634	NA	−9.9	NA	Age determination	22
VM29-84	LGM	Determined in publication	NA	NA	0.7125000	NA	NA	NA	Age – LGM	24
VM29-86	LGM	Determined in publication	NA	NA	0.7085000	NA	NA	NA	Age – LGM	
VM29-89	LGM	Determined in publication	NA	NA	0.7123800	NA	NA	NA	Age – LGM	18
VM29-90	LGM	Determined in publication	NA	NA	0.7138900	NA	NA	NA	Age – LGM	
VM30-41K	LGM	Determined in publication	NA		0.71747		−11.40		Age – LGM	22
VM34-153	LGM	Determined in publication	NA	NA	0.7183000	NA	NA	NA	Age – LGM	
VM34-155	LGM	Determined in publication	NA	NA	0.7188800	NA	NA	NA	Age – LGM	18
VM34-156	LGM	Determined in publication	NA	NA	0.7189000	NA	NA	NA	Age – LGM	
VM34-157	LGM	Determined in publication	NA	NA	0.7177400	NA	NA	NA	Age – LGM	24
VM34-158	LGM	Determined in publication	NA	NA	0.7188000	NA	NA	NA	Age – LGM	18
Lake Eyre	∼ 65 ka	Determined in publication	NA	NA	0.709867	NA	−4	NA	Age	16
64PE349-8	S3	240	83.94	2	0.71427	0.00066	−11.31	0.21	visual, geochemical (TOC, Ba/Al)	
64PE349-8	S4	280–300	102.46–110.66	4	0.71499	0.00168	−9.85	1.70	visual, geochemical (TOC, Ba/Al)	2
64PE349-8	S5	345–375	126.81–138.83	6	0.71518	0.00112	−11.02	0.66	visual, geochemical (TOC, Ba/Al)	
KL83	S5	398–414		4	0.70931	0.00003	−5.13	0.19	visual, geochemical ($\delta^{18}O$)	
SL67	S5	386.5–446.5	NA	4	0.71039	0.00024	−7.45	0.06	visual, geochemical ($\delta^{18}O$)	
SL71	S5	263–275.5	NA	4	0.71129	0.00074	−8.00	0.50	visual, geochemical ($\delta^{18}O$)	25
KL51	S6	535.5–573.5		4	0.71164	0.00042	−7.98	0.28	visual, geochemical ($\delta^{18}O$)	
KL83	S6	566–618		6	0.70907	0.00019	−4.20	0.25	visual, geochemical ($\delta^{18}O$)	
SL71	S6	387.5–4145	NA	4	0.71231	0.00075	−8.58	0.75	visual, geochemical ($\delta^{18}O$)	

NA: not available.

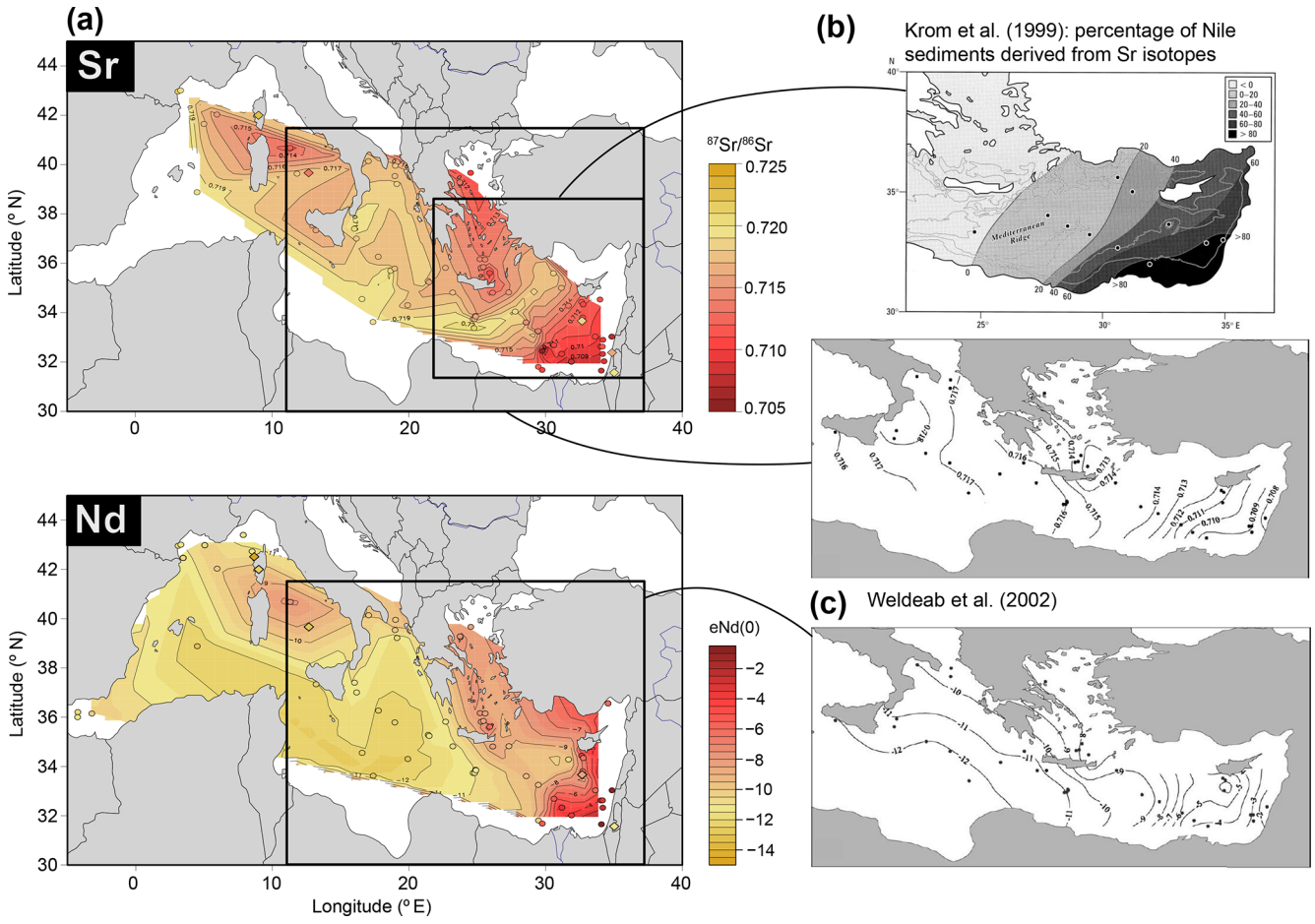

Figure 2. Contour maps of the isotopic signature of marine surface sediments in the Mediterranean. **(a)** Contour maps produced using the assembled dataset for strontium and neodymium isotopes. The contour lines and filled contour maps were realized using individual surface (or core-top) sediment samples. Each sample is represented by a dot whose colour indicates its isotopic value according to the scale at the right of the panels. Aerosol samples are overlaid and represented by a diamond with a similar colour code. These maps are compared to previous contour maps from Krom et al. (1999b) (where the Sr isotopes calculate a percentage of surface sediments derived from the Nile River runoff) **(b)** and Weldeab et al. (2002a) **(c)**, which were inspirational to this work. Their respective extent is reported on the maps in **(a)**.

tained average and standard deviation (2σ) values, are reported in Table 2.

– Labelled "LGM" (Last Glacial Maximum): samples of Last Glacial Maximum age (i.e. ca. 20–25 ka BP) that were clearly identified in the original references were also added to the database. Related depth intervals and averaged values were determined in the cited publications (see Table 2).

3 Results

The dataset assembled includes the following fields for each sample:

– name of the sample or sediment core;

– criteria for location: region, sub-region, location;

– sample type: soil sediment, river sediment, marine sediment, aerosol, trap sample, rocks;

– grain-size fraction on which the measurements were made;

– criteria for time interval: present, sapropel layers, Last Glacial Maximum, or others as specified in the original publication;

– concentration and isotopic ratio in strontium and/or neodymium;

– geographical coordinates: original longitude and latitude (from the reference publication) and longitude and latitude (in decimal degrees), as well as notes on coordinates;

– notes on sample: specific information about the sample (from the reference publication);

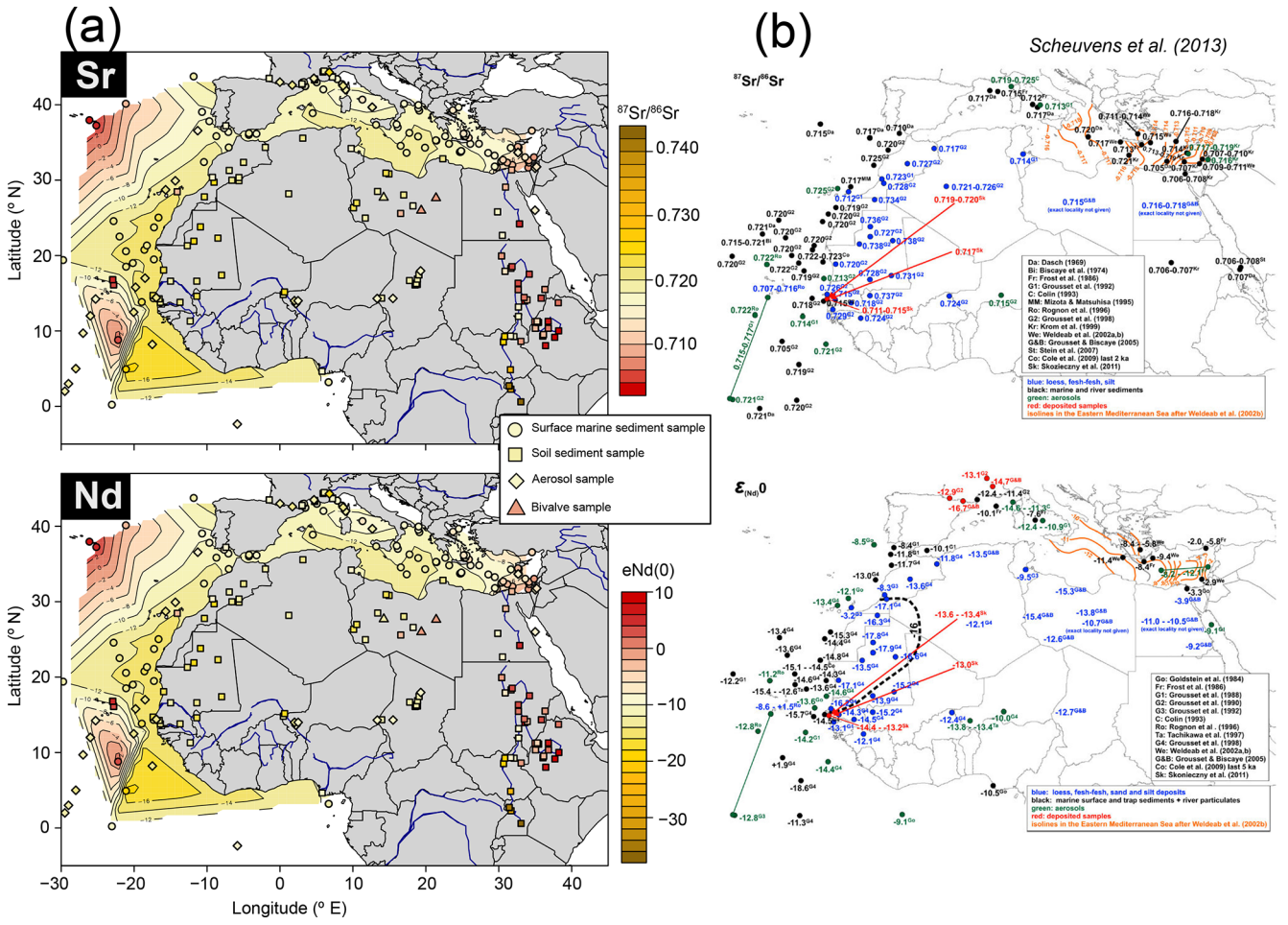

Figure 3. Contour maps of the isotopic signature of marine and terrestrial sediment in the northern African sector realized using the first iteration of the database (September 2018). **(a)** Comparison of the isotopic signature of marine surface sediments (contour maps) to that of terrestrial samples. Sample type is indicated by specific markers, whose colour indicates its isotopic value according to the scale to the right of the panels: dots for marine surface sediments, squares for terrestrial (soil and river) sediment samples, and diamonds for aerosols and triangles for fossil bivalves. **(b)** Maps from Scheuvens et al. (2013), which were inspirational to this work. The sample type is given by the colour of the markers: blue for terrestrial samples, black for marine samples, green for aerosols (sediment traps) and red for deposited samples. Isotopic values are reported for each sample and the isolines from Weldeab et al. (2002b; cf. Fig. 3) are also reported.

- reference: original reference publication of the sample;
- date of contribution: when the sample was added to the database; and
- source: origin of the data point: literature search, own (own measurements), author contribution, external contribution, sedDB (from the Sed database, http://www.earthchem.org/seddb, last access: 20 February 2019), Scheuvens et al. (2013), Padoan et al. (2011), Jeandel et al. (2007) (see Sect. 2.1).

Table 3 provides an overview of the number of samples in the various categories defined in Sect. 2.2. Most samples are located in Africa, the Atlantic Ocean and the Indian Ocean and represent the present-day sedimentation patterns. Most of the samples in the database are marine sediments, while there is also a significant contribution from river and soil sediments.

The sorting criterion allows users to select only a subset of the data and to map the isotopic values (see Figs. 2 and 3). As an example, samples originating from various PSAs in Africa are reported in Table 3 and will be used to fingerprint PSAs based on their isotopic signature and standard statistical methods (see Fig. 4).

4 Technical validation

As the database is built by incrementing new measurements and homogenizing the metadata, one way to check its validity is to compare it with previously published compilations.

Table 3. Soil and river samples located in the African PSA (potential source area for dust generation). Headers from left to right: Label: name of the sampling location or sample; Region: country where the samples were taken; Location: name of the PSA (see Fig. 1); Sample type: soil or river sediment; Isotopic ratios of Sr and Nd; Longitude and Latitude (decimal degrees); Ref.: reference publications. These data were used to determine and plot the statistical values in Fig. 4. References: 1: Grousset et al. (1992), 2: Grousset and Biscaye (2005), 3: Grousset et al. (1998), 4: Gross et al. (2016), 5: Revel et al. (2010), 6: Abouchami et al. (2013), 7: Krom et al. (2002), 8: Padoan et al. (2011).

Label	Sub-region	Location	Sample type	$^{87}Sr/^{86}Sr$	$\varepsilon_{Nd(0)}$	Longitude (dec. degrees)	Latitude (dec. degrees)	Ref.
TUI78	Tunisia	PSA1	soil sediment	0.71424	−9.5	9.78	34.20	1
Algeria	Algeria	PSA1	soil sediment		−13.5	3.14	35.57	2
Senegal River	Senegal	PSA2	river sediment	0.72858	−13.1	−15.00	16.60	
Kiffa	Mauritania	PSA2	soil sediment	0.72839	−13.9	−11.40	16.60	
Nouakchott	Mauritania	PSA2	soil sediment	0.72002	−15.9	−15.95	18.07	
Erg Sud Atar	Mauritania	PSA2	soil sediment	0.73765	−13.5	−12.70	21.30	3
Atar	Mauritania	PSA2	soil sediment	0.72728	−17.9	−11.80	21.90	
Zouerat	Mauritania	PSA2	soil sediment	0.73568	−17.8	−10.90	23.80	
Essmarra	Morocco	PSA2	soil sediment	0.73404	−16.3	−10.36	27.78	
JB	Moroco	PSA2	soil sediment	0.72194	−14.0	−5.62	29.93	
IR	Morocco	PSA2	soil sediment	0.72565	−13.8	−6.58	29.98	4
EM	Morocco	PSA2	soil sediment	0.72764	−13.0	−5.62	30.35	
ATK-35 (Atakor)	Algeria	PSA3	soil sediment		−12.1	1.21	28.19	
MEK-21 (Sebkra Mekkerane)	Algeria	PSA3	soil sediment	0.72052		1.66	28.03	3
MEK-58 (Sebkra Mekkerane)	Algeria	PSA3	soil sediment	0.72440		1.66	28.03	
Libya2	Libya	PSA4	soil sediment		−13.8	16.98	28.03	2
Libya4	Libya	PSA4	soil sediment	0.71521	−10.7	18.26	26.59	2
N26	Libya	PSA4	soil sediment	0.70651	−3.8	16.57	25.58	5
Chad	Chad	PSA5	soil sediment		−12.7	13.95	14.35	2
Bod 43.5	Chad	PSA5	soil sediment		−13.1	18.55	16.10	
Bod 43.5_duplicate	Chad	PSA5	soil sediment	0.72833	−12.7	18.55	16.10	
Bod 44	Chad	PSA5	soil sediment	0.71498	−10.2	18.84	16.17	
Bod 44B	Chad	PSA5	soil sediment	0.71477	−10.1	18.84	16.17	
Bod 54A	Chad	PSA5	soil sediment	0.72908	−13.1	18.61	16.20	
Bod 54A_duplicate	Chad	PSA5	soil sediment	0.72931	−12.7	18.61	16.20	6
Bod 54B	Chad	PSA5	soil sediment		−12.8	18.61	16.20	
Bod 54B_duplicate	Chad	PSA5	soil sediment	0.72761	−12.9	18.61	16.20	
Bod 44C	Chad	PSA5	soil sediment		−13.0	18.71	16.29	
Bod 44D	Chad	PSA5	soil sediment	0.72794		18.71	16.29	
Bod 44D_duplicate	Chad	PSA5	soil sediment	0.72791	−12.9	18.71	16.29	

Table 3. Continued.

Label	Sub-region	Location	Sample type	$^{87}Sr/^{86}Sr$	$\varepsilon_{Nd(0)}$	Longitude (dec. degrees)	Latitude (dec. degrees)	Ref.
BODI	Chad	PSA5	soil sediment	0.71858	−11.9	17.78	16.68	4
BODU	Chad	PSA5	soil sediment	0.71785	−12.6	18.87	16.87	4
Bod 51	Chad	PSA5	soil sediment		−12.2	19.07	17.43	6
Bod 51_duplicate	Chad	PSA5	soil sediment	0.72129	−12.0	19.07	17.43	6
Sudan	Sudan	PSA6	river sediment	0.70567		28.66	20.92	7
Sudan	Sudan	PSA6	river sediment	0.70661		28.66	20.92	7
Main Nile, 3rd cataract	Sudan	PSA6	river sediment	0.70497	1.7	30.41	19.94	
Main Nile, 3rd cataract	Sudan	PSA6	river sediment	0.70536		30.41	19.94	8
Main Nile, 3rd cataract	Sudan	PSA6	river sediment	0.70614	−0.8	30.41	19.94	
Main Nile, 3rd cataract	Sudan	PSA6	river sediment	0.70591		30.41	19.94	
Egypt1	Egypt	PSA6	soil sediment		−9.2	30.52	22.67	2
Main Nile, Ghaba	Sudan	PSA6	river sediment	0.70516		30.75	18.14	
Main Nile, Ghaba	Sudan	PSA6	river sediment	0.70508		30.75	18.14	
W. Milk, Ed Debba	Sudan	PSA6	river sediment	0.70743	−7.5	30.89	17.91	
W. Milk, Ed Debba	Sudan	PSA6	river sediment	0.70694		30.89	17.91	
W. Milk, Ed Debba	Sudan	PSA6	river sediment	0.71563	−7.3	30.89	17.91	
W. Milk, Ed Debba	Sudan	PSA6	river sediment	0.71691		30.89	17.91	
Main Nile, Gureir	Sudan	PSA6	river sediment	0.70526	−2.9	31.69	18.31	
Main Nile, Gureir	Sudan	PSA6	river sediment	0.70507		31.69	18.31	
Main Nile, Karima	Sudan	PSA6	river sediment	0.70469	1.2	31.85	18.53	8
Main Nile, Karima	Sudan	PSA6	river sediment	0.70506		31.85	18.53	
Nile, 6th cataract	Sudan	PSA6	river sediment	0.70546	1.2	32.69	16.33	
Nile, 6th cataract	Sudan	PSA6	river sediment	0.70566		32.69	16.33	
Blue Nile, Khartoum	Sudan	PSA6	river sediment	0.70513	0.7	32.70	15.47	
Blue Nile, Khartoum	Sudan	PSA6	river sediment	0.70546		32.70	15.47	
Blue Nile, Khartoum	Sudan	PSA6	river sediment	0.70516	0.7	32.70	15.47	
Assouan_bank	Egypt	PSA6	river sediment	0.70594	−3.4	32.88	24.20	5
Assouan_island	Egypt	PSA6	river sediment	0.70580	3.4	32.88	24.20	5
Blue Nile, Wad Madani	Sudan	PSA6	river sediment		−0.3	33.50	14.44	
Blue Nile, Wad Madani	Sudan	PSA6	river sediment	0.70551		33.50	14.44	
Atbara, Abu Ammar	Sudan	PSA6	river sediment	0.70433	2.3	34.21	17.53	
Atbara, Abu Ammar	Sudan	PSA6	river sediment	0.70470		34.21	17.53	8
Derudeb, Derudeb	Ethiopia	PSA6	river sediment	0.70504		36.12	17.98	
Gash, Kassala	Sudan	PSA6	river sediment	0.70513	−4.2	36.36	15.50	
Gash, Kassala	Sudan	PSA6	river sediment	0.70496		36.36	15.50	
Gash, Kassala	Sudan	PSA6	river sediment	0.70577	−2.4	36.36	15.50	

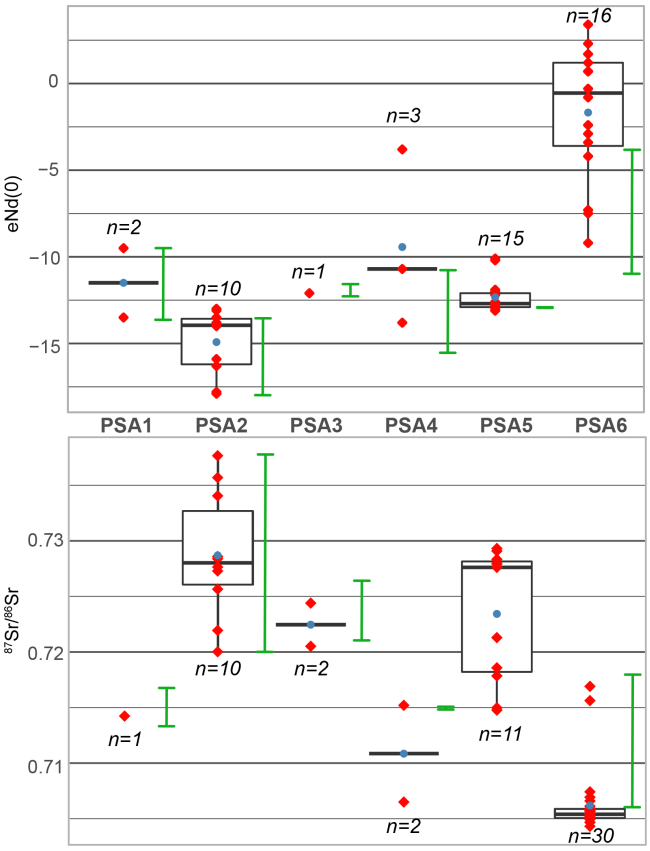

Figure 4. Box and whiskers plot for the isotopic signatures of African PSAs. After identifying samples that are located in each PSA (see Table 3 and Fig. 1), the range and skewness of datasets in the PSA were analysed using box and whiskers plots (when sample number n was higher than 5) and compared to the isotopic ranges reported by Scheuvens et al. (2013) (green bars). Data points are shown as red diamonds and the arithmetical mean is provided (blue dots). The rectangles indicate the upper and lower quartiles and the median is shown as a thicker horizontal line (Krzywinski and Altman, 2014).

Some of the earlier works that inspired and motivated this exercise are the mapping of Sr and Nd isotopes in seafloor sediments in the Mediterranean Sea by Krom et al. (1999b) and Weldeab et al. (2002a). These studies were innovative and provided a clear illustration of the role of continental sediment sources and land-to-sea transportation as well as submarine currents in building sedimentary deposits. It also highlighted the importance of accurately reconstructing present-day sedimentary dynamics to interpret the geological record. Both studies being (almost) 20 years old, the initial intention was to update their data compilation to integrate new measurements and generate more detailed maps of seafloor sediment signatures. The comparisons between the original maps and new maps based on the database are presented in Fig. 2. If the general pattern already identified by both studies (i.e. the large influence of Nile-derived sediment input on the eastern Levantine Basin) is reproduced by the new compilation, it allows the extension of the record to the western part of the basin and unravels some new features. For instance, the updated maps demonstrate the influence of runoff from the Aegean sub-basin and the large impact of dust delivery on the Ionian sub-basin (with perhaps some local runoff from the Syrian and Tunisian coasts). Not shown here, the compilation and addition of sapropel layers also allow us to map the effect of the increase in river runoff on the sedimentary signature of seafloor sediments.

Another motivation to build this database is the recent publication by Scheuvens et al. (2013), which provides a synoptic view of the geochemical signatures of African PSAs for dust generation. In particular, this study compiled a large number of data for Nd and Sr radioisotopes from soils, aerosols and marine sediments. The present database largely builds on the compilation by Scheuvens et al. (2013), which has been homogenized and completed with recent measurements, especially the Nile River sedimentary data from Padoan et al. (2011). One of the main modifications that was implemented is that approximate coordinates were attributed to samples with no given coordinate in the original reference. This was realized by using all available information, e.g. mention of cities or locations in the sample label or sample description, or approximate location from the published maps (see Sect. 2.2). This operation was realized with great care as this is the main source of error and is clearly indicated in the database. It is however an important step as it allows us to map contour lines that help in unravelling features associated with earth-surface processes (dust transportation, river runoff) that cannot be readily identified on maps in Scheuvens et al. (2013) (Fig. 3).

The validity of the approach was controlled by comparing the values provided in Scheuvens et al. (2013) for the African PSAs to those computed using the present dataset (Fig. 4). Overall, the values obtained for each PSA are in good agreement with previous estimations. The integration of additional samples allowed us to either confirm the observed values (e.g. for PSA1, PSA2 and PSA3) or to extend the value range and the number of data points (e.g. for PSA4, PSA5 and PSA6). One further advantage of using sorting criteria is that it allows us to determine and plot statistics values associated with the PSA (Fig. 4). When the number of samples was higher than 5, the data range was depicted as box plots, which allow us to determine the skewness of the data (i.e. by looking at the difference between the mean in blue and the median, which is represented as the bar in the rectangles) (Krzywinski and Altman, 2014). The presence of outliers like in the Sr signature of PSA6 can be identified and dismissed from the source fingerprinting.

Table 4. Output table after second iteration (April 2019). Overview of the results obtained in number of data points per type of sample, time interval and location of the samples (Af: Africa, Am: America, Ant: Antarctica, Arct O: Artctic Ocean, Asia, Atl O: Atlantic Ocean, Aus: Australia, Eur: Europe, Green: Greenland, Ind O: Indian Ocean, South O: Southern Ocean, Medit S: Mediterranean Sea, Pac O: Pacific Ocean).

	Time int.	Af	Am	Ant	Arct O	Asia	Atl O	Aus	Eur	Green	Ind O	South O	Medit S	Pac O	Total
aerosol	P	29	8	14		22	35	4	7	6			18	3	147
bivalves	P	3													3
	LGM	1					55	1			55	5		9	126
	P	8	9	2	39	8	208	2	3		130	42	74	64	589
	S1	3					1				1		21		26
marine	S3												1		1
sediment	S4												1		1
	S5												4		4
	S6												3		3
	Other							1							1
river	P	131	23			23	5	7	56						245
sediment	S1												1		1
Rocks	P	45	17	3		15	16	6	5	1	8	3		12	131
soil	P	81	24			88	10	14	2		1	1			221
sediment	LGM							2							2
	Other							2							2
trap sample	P						9						20		29
Total		301	81	19	39	156	339	39	73	7	196	51	144	88	1533

5 Code and data availability

The dataset of neodymium and strontium isotope ratios and the associated metadata table, as well as Table 2 (determination of isotopic signature and identification of specific time intervals) and the associated metadata table, are available at https://doi.org/10.5880/GFZ.4.3.2019.001 (Blanchet, 2019). The dataset and associated metadata are stored at the GFZ Data Service as comma-separated files, but they can also be provided as an Excel file upon request.

All figures were realized using the R freeware (R Core Team, 2013) and packages "marmap" (Pante and Simon-Bouhet, 2013) and "ggplot2" (Wickham, 2016). The R codes to reproduce maps in Figs. 1, 2 and 3 as well as the box and whiskers plots in Fig. 4 are available on Figshare (Blanchet, 2018a, b).

6 Conclusion and outlook

The dataset assembled and presented here provides new insights into present and past earth-surface processes and the building of the marine sedimentary record. It allows us to compare various types of sediments from the terrestrial to marine realms: soils, deposited dust, river sediments, rocks, bivalves or marine sediments (Table 4). The attribution of standardized geolocations enables us to map the data and therefore to visualize sedimentary dynamics, while the use of sorting criteria related to the sample location or depositional age permits us to determine source and sink isotopic signatures using statistical methods.

This database is thought of as an evolving tool and is intended to grow as new measurements are published or provided by peers. Users are encouraged to contact the author (who will act as a curator) to submit new data and/or to propose any modification or improvement of the database. With that aim, an indication of the entry date is provided, which will help users to follow the database updates and versions.

Competing interests. The author declares that they have no conflict of interest.

Acknowledgements. I would like to acknowledge the financial support of the Free University Berlin and the GFZ Potsdam. The valuable help of Kirsten Elger and Boris Radosavljevic from the GFZ Data Service was instrumental in getting the dataset ready for publication. Both dedicated a lot of time and patience, for which I am very grateful. Constructive comments by Michael D. Krom and an anonymous reviewer are also gratefully acknowledged.

Review statement. This paper was edited by David Carlson and reviewed by Michael Krom and one anonymous referee.

References

Abouchami, W., Näthe, K., Kumar, A., Galer, S. J. G., Jochum, K. P., Williams, E., Horbe, A. M. C., Rosa, J. W. C., Balsam, W., Adams, D., Mezger, K., and Andreae, M. O.: Geochemical and isotopic characterization of the Bodélé Depression dust source and implications for transatlantic dust transport to the Amazon Basin, Earth Planet. Sc. Lett., 380, 112–123, https://doi.org/10.1016/j.epsl.2013.08.028, 2013.

Blanchet, C.: R Code for mapping (contour maps) the Nd and Sr isotopic signature of marine and terrestrial sediments, figshare, https://doi.org/10.6084/m9.figshare.6990161.v3, 2018a.

Blanchet, C.: R Code for plotting statistical parameters of Nd and Sr isotopic signature of Potential Source Areas, figshare, https://doi.org/10.6084/m9.figshare.6990260.v3, 2018b.

Blanchet, C. L.: A global database of radiogenic Nd and Sr isotopes in marine and terrestrial samples (V. 2.0), available at: http://dataservices.gfz-potsdam.de/panmetaworks/showshort.php?id=escidoc:4094893, last access: 13 May 2019.

Blanchet, C. L., Tjallingii, R., Frank, M., Lorenzen, J., Reitz, A., Brown, K., Feseker, T., and Brückmann, W.: High- and low-latitude forcing of the Nile River regime during the Holocene inferred from laminated sediments of the Nile deep-sea fan, Earth Planet. Sc. Lett., 364, 98–110, https://doi.org/10.1016/j.epsl.2013.01.009, 2013.

Blanchet, C. L., Frank, M., and Schouten, S.: Asynchronous Changes in Vegetation, Runoff and Erosion in the Nile River Watershed during the Holocene, PLOS ONE, 9, e115958, https://doi.org/10.1371/journal.pone.0115958, 2014.

Bouvier, A., Vervoort, J. D., and Patchett, P. J.: The Lu–Hf and Sm–Nd isotopic composition of CHUR: Constraints from unequilibrated chondrites and implications for the bulk composition of terrestrial planets, Earth Planet. Sc. Lett., 273, 48–57, https://doi.org/10.1016/j.epsl.2008.06.010, 2008.

Box, M. R., Krom, M. D., Cliff, R. A., Bar-Matthews, M., Almogi-Labin, A., Ayalon, A., and Paterne, M.: Response of the Nile and its catchment to millennial-scale climatic change since the LGM from Sr isotopes and major elements of East Mediterranean sediments, Quaternary Sci. Rev., 30, 431–442, https://doi.org/10.1016/j.quascirev.2010.12.005, 2011.

Castañeda, I. S., Schouten, S., Pätzold, J., Lucassen, F., Kasemann, S., Kuhlmann, H., and Schefuß, E.: Hydroclimate variability in the Nile River Basin during the past 28,000 years, Earth Planet. Sc. Lett., 438, 47–56, https://doi.org/10.1016/j.epsl.2015.12.014, 2016.

Cole, J. M., Goldstein, S. L., deMenocal, P. B., Hemming, S. R., and Grousset, F. E.: Contrasting compositions of Saharan dust in the eastern Atlantic Ocean during the last deglaciation and African Humid Period, Earth Planet. Sc. Lett., 278, 257–266, https://doi.org/10.1016/j.epsl.2008.12.011, 2009.

Colin, C., Turpin, L., Bertaux, J., Desprairies, A., and Kissel, C.: Erosional history of the Himalayan and Burman ranges during the last two glacial–interglacial cycles, Earth Planet. Sc. Lett., 171, 647–660, https://doi.org/10.1016/S0012-821X(99)00184-3, 1999.

De Lange, G. J., Thomson, J., Reitz, A., Slomp, C. P., Speranza Principato, M., Erba, E., and Corselli, C.: Synchronous basin-wide formation and redox-controlled preservation of a Mediterranean sapropel, Nat. Geosci., 1, 606–610, https://doi.org/10.1038/ngeo283, 2008.

Frank, M.: Radiogenic isotopes: Tracers of past ocean circulation and erosional input, Rev. Geophys., 40, 1-1–1-38, https://doi.org/10.1029/2000RG000094, 2002.

Franzese, A. M., Hemming, S. R., Goldstein, S. L., and Anderson, R. F.: Reduced Agulhas Leakage during the Last Glacial Maximum inferred from an integrated provenance and flux study, Earth Planet. Sc. Lett., 250, 72–88, https://doi.org/10.1016/j.epsl.2006.07.002, 2006.

Franzese, A. M., Hemming, S. R., and Goldstein, S. L.: Use of strontium isotopes in detrital sediments to constrain the glacial position of the Agulhas Retroflection, Paleoceanography, 24, PA2217, https://doi.org/10.1029/2008PA001706, 2009.

Freydier, R., Michard, A., De Lange, G., and Thomson, J.: Nd isotopic compositions of Eastern Mediterranean sediments: tracers of the Nile influence during sapropel S1 formation?, Mar. Geol., 177, 45–62, https://doi.org/10.1016/S0025-3227(01)00123-2, 2001.

Goldstein, S. L. and O'Nions, R. K.: Nd and Sr isotopic relationships in pelagic clays and ferromanganese deposits, Nature, 292, 324–327, https://doi.org/10.1038/292324a0, 1981.

Goldstein, S. L., O'Nions, R. K., and Hamilton, P. J.: A Sm-Nd isotopic study of atmospheric dusts and particulates from major river systems, Earth Planet. Sc. Lett., 70, 221–236, https://doi.org/10.1016/0012-821X(84)90007-4, 1984.

Gross, A., Palchan, D., Krom, M. D., and Angert, A.: Elemental and isotopic composition of surface soils from key Saharan dust sources, Chem. Geol., 442, 54–61, https://doi.org/10.1016/j.chemgeo.2016.09.001, 2016.

Grousset, F. E. and Biscaye, P. E.: Tracing dust sources and transport patterns using Sr, Nd and Pb isotopes, Chem. Geol., 222, 149–167, https://doi.org/10.1016/j.chemgeo.2005.05.006, 2005.

Grousset, F. E., Biscaye, P. E., Zindler, A., Prospero, J., and Chester, R.: Neodymium isotopes as tracers in marine sediments and aerosols: North Atlantic, Earth Planet. Sc. Lett., 87, 367–378, https://doi.org/10.1016/0012-821X(88)90001-5, 1988.

Grousset, F. E., Henry, F., Minster, J. F., and Monaco, A.: Nd isotopes as tracers in water column particles: the western Mediterranean Sea, Mar. Chem., 30, 389–407, https://doi.org/10.1016/0304-4203(90)90083-O, 1990.

Grousset, F. E., Rognon, P., Coudé-Gaussen, G., and Pédemay, P.: Origins of peri-Saharan dust deposits traced by their Nd and Sr isotopic composition, Palaeogeogr. Palaeocl., 93, 203–212, https://doi.org/10.1016/0031-0182(92)90097-O, 1992.

Grousset, F. E., Parra, M., Bory, A., Martinez, P., Bertrand, P., Shimmield, G., and Ellam, R. M.: Saharan wind regimes traced by the Sr–Nd isotopic composition of subtropical Atlantic sediments: last glacial maximum vs today, Quaternary Sci. Rev., 17, 395–409, https://doi.org/10.1016/S0277-3791(97)00048-6, 1998.

Hemming, S. R., Flierdt, T. van de, Goldstein, S. L., Franzese, A. M., Roy, M., Gastineau, G., and Landrot, G.: Strontium isotope tracing of terrigenous sediment dispersal in the Antarctic Circumpolar Current: Implications for constraining frontal positions, Geochem. Geophy. Geosy., 8, Q06N13, https://doi.org/10.1029/2006GC001441, 2007.

Jacobsen, S. B. and Wasserburg, G. J.: Sm–Nd isotopic evolution of chondrites, Earth Planet. Sc. Lett., 50, 139–155, https://doi.org/10.1016/0012-821X(80)90125-9, 1980.

Jeandel, C., Arsouze, T., Lacan, F., Téchiné, P. and Dutay, J.-C.: Isotopic Nd compositions and concentrations of the lithogenic inputs into the ocean: A compilation, with an emphasis on the margins, Chem. Geol., 239, 156–164, https://doi.org/10.1016/j.chemgeo.2006.11.013, 2007.

Jung, S. J. A., Davies, G. R., Ganssen, G. M., and Kroon, D.: Stepwise Holocene aridification in NE Africa deduced from dust-borne radiogenic isotope records, Earth Planet. Sc. Lett., 221, 27–37, https://doi.org/10.1016/S0012-821X(04)00095-0, 2004.

Krom, M. D., Michard, A., Cliff, R. A., and Strohle, K.: Sources of sediment to the Ionian Sea and western Levantine basin of the Eastern Mediterranean during S-1 sapropel times, Mar. Geol., 160, 45–61, https://doi.org/10.1016/S0025-3227(99)00015-8, 1999a.

Krom, M. D., Cliff, R. A., Eijsink, L. M., Herut, B., and Chester, R.: The characterisation of Saharan dusts and Nile particulate matter in surface sediments from the Levantine basin using Sr isotopes, Mar. Geol., 155, 319–330, https://doi.org/10.1016/S0025-3227(98)00130-3, 1999b.

Krom, M. D., Stanley, J. D., Cliff, R. A., and Woodward, J. C.: Nile River sediment fluctuations over the past 7000 yr and their key role in sapropel development, Geology, 30, 71, https://doi.org/10.1130/0091-7613(2002)030<0071:NRSFOT>2.0.CO;2, 2002.

Krzywinski, M. and Altman, N.: Points of Significance: Visualizing samples with box plots, Nat. Methods, 11, 119–120, https://doi.org/10.1038/nmeth.2813, 2014.

Noble, T. L., Piotrowski, A. M., Robinson, L. F., McManus, J. F., Hillenbrand, C.-D., and Bory, A. J.-M.: Greater supply of Patagonian-sourced detritus and transport by the ACC to the Atlantic sector of the Southern Ocean during the last glacial period, Earth Planet. Sc. Lett., 317–318, 374–385, https://doi.org/10.1016/j.epsl.2011.10.007, 2012.

Osborne, A. H., Vance, D., Rohling, E. J., Barton, N., Rogerson, M., and Fello, N.: A humid corridor across the Sahara for the migration of early modern humans out of Africa 120,000 years ago, P. Natl. Acad. Sci. USA, 105, 16444–16447, https://doi.org/10.1073/pnas.0804472105, 2008.

Padoan, M., Garzanti, E., Harlavan, Y., and Villa, I. M.: Tracing Nile sediment sources by Sr and Nd isotope signatures (Uganda, Ethiopia, Sudan), Geochim. Cosmochim. Act. 75, 3627–3644, https://doi.org/10.1016/j.gca.2011.03.042, 2011.

Palchan, D., Stein, M., Almogi-Labin, A., Erel, Y., and Goldstein, S. L.: Dust transport and synoptic conditions over the Sahara–Arabia deserts during the MIS6/5 and 2/1 transitions from grain-size, chemical and isotopic properties of Red Sea cores, Earth Planet. Sc. Lett., 382, 125–139, https://doi.org/10.1016/j.epsl.2013.09.013, 2013.

Pante, E. and Simon-Bouhet, B.: marmap: A Package for Importing, Plotting and Analyzing Bathymetric and Topographic Data in R, PLOS ONE, 8, e73051, https://doi.org/10.1371/journal.pone.0073051, 2013.

R Core Team: R: A language and environment for statistical computing, R Foundation for Statistical Computing, Vienna, Austria, available at: http://www.R-project.org/ (last access: 20 February 2019), 2013.

Revel, M., Sinko, J. A., Grousset, F. E., and Biscaye, P. E.: Sr and Nd isotopes as tracers of North Atlantic lithic particles: Paleoclimatic implications, Paleoceanography, 11, 95–113, https://doi.org/10.1029/95PA03199, 1996.

Revel, M., Ducassou, E., Grousset, F. E., Bernasconi, S. M., Migeon, S., Revillon, S., Mascle, J., Murat, A., Zaragosi, S., and Bosch, D.: 100,000 Years of African monsoon variability recorded in sediments of the Nile margin, Quaternary Sci. Rev., 29, 1342–1362, https://doi.org/10.1016/j.quascirev.2010.02.006, 2010.

Revel, M., Colin, C., Bernasconi, S., Combourieu-Nebout, N., Ducassou, E., Grousset, F. E., Rolland, Y., Migeon, S., Bosch, D., Brunet, P., Zhao, Y., and Mascle, J.: 21,000 Years of Ethiopian African monsoon variability recorded in sediments of the western Nile deep-sea fan, Reg. Environ. Change, 14, 1685–1696, https://doi.org/10.1007/s10113-014-0588-x, 2014.

Revel, M., Ducassou, E., Skonieczny, C., Colin, C., Bastian, L., Bosch, D., Migeon, S., and Mascle, J.: 20,000 years of Nile River dynamics and environmental changes in the Nile catchment area as inferred from Nile upper continental slope sediments, Quaternary Sci. Rev., 130, 200–221, https://doi.org/10.1016/j.quascirev.2015.10.030, 2015.

Revel-Rolland, M., De Deckker, P., Delmonte, B., Hesse, P. P., Magee, J. W., Basile-Doelsch, I., Grousset, F., and Bosch, D.: Eastern Australia: A possible source of dust in East Antarctica interglacial ice, Earth Planet. Sc. Lett., 249, 1–13, https://doi.org/10.1016/j.epsl.2006.06.028, 2006.

Révillon, S., Jouet, G., Bayon, G., Rabineau, M., Dennielou, B., Hémond, C., and Berné, S.: The provenance of sediments in the Gulf of Lions, western Mediterranean Sea, Geochem. Geophy. Geosy., 12, Q08006, https://doi.org/10.1029/2011GC003523, 2011.

Rossignol-Strick, M.: Mediterranean Quaternary sapropels, an immediate response of the African monsoon to variation of insolation, Palaeogeogr. Palaeocl., 49, 237–263, https://doi.org/10.1016/0031-0182(85)90056-2, 1985.

Roy, M., van de Flierdt, T., Hemming, S. R., and Goldstein, S. L.: $^{40}Ar/^{39}Ar$ ages of hornblende grains and bulk Sm/Nd isotopes of circum-Antarctic glacio-marine sediments: Implications for sediment provenance in the southern ocean, Chem. Geol., 244, 507–519, https://doi.org/10.1016/j.chemgeo.2007.07.017, 2007.

Scheuvens, D., Schütz, L., Kandler, K., Ebert, M., and Weinbruch, S.: Bulk composition of northern African dust and its source sediments – A compilation, Earth-Sci. Rev., 116, 170–194, https://doi.org/10.1016/j.earscirev.2012.08.005, 2013.

Stein, M., Almogi-Labin, A., Goldstein, S. L., Hemleben, C., and Starinsky, A.: Late Quaternary changes in desert dust inputs to the Red Sea and Gulf of Aden from 87Sr/86Sr ratios in deep-sea cores, Earth Planet. Sc. Lett., 261, 104–119, https://doi.org/10.1016/j.epsl.2007.06.008, 2007.

Tachikawa, K., Arsouze, T., Bayon, G., Bory, A., Colin, C., Dutay, J.-C., Frank, N., Giraud, X., Gourlan, A. T., Jeandel, C., Lacan, F., Meynadier, L., Montagna, P., Piotrowski, A. M., Plancherel, Y., Pucéat, E., Roy-Barman, M., and Waelbroeck, C.: The large-scale evolution of neodymium isotopic composition in the global modern and Holocene ocean revealed from seawater and archive data, Chem. Geol., 457, 131–148, https://doi.org/10.1016/j.chemgeo.2017.03.018, 2017.

Weldeab, S., Emeis, K.-C., Hemleben, C., and Siebel, W.: Provenance of lithogenic surface sediments and pathways of riverine suspended matter in the Eastern Mediterranean Sea: evidence from $^{143}Nd/^{144}Nd$ and $^{87}Sr/^{86}Sr$ ratios, Chem. Geol., 186, 139–149, https://doi.org/10.1016/S0009-2541(01)00415-6, 2002a.

Weldeab, S., Emeis, K.-C., Hemleben, C., Vennemann, T. W., and Schulz, H.: Sr and Nd isotope composition of Late Pleistocene sapropels and nonsapropelic sediments from the Eastern Mediterranean Sea: implications for detrital influx and climatic conditions in the source areas, Geochim. Cosmochim. Ac., 66, 3585–3598, https://doi.org/10.1016/S0016-7037(02)00954-7, 2002b.

Wickham, H.: ggplot2: Elegant Graphics for Data Analysis, Springer-Verlag New York, available at: http://ggplot2.org (last access: 20 February 2019), 2016.

Wu, J., Böning, P., Pahnke, K., Tachikawa, K., and de Lange, G. J.: Unraveling North-African riverine and eolian contributions to central Mediterranean sediments during Holocene sapropel S1 formation, Quaternary Sci. Rev., 152, 31–48, https://doi.org/10.1016/j.quascirev.2016.09.029, 2016.